HAL
open science

Importance of endogenous extracellular matrix in biomechanical properties of human skin model

Flavien Pillet, Laure Gibot, Moinecha Madi, Marie-Pierre Rols, Etienne Dague

To cite this version:

Flavien Pillet, Laure Gibot, Moinecha Madi, Marie-Pierre Rols, Etienne Dague. Importance of endogenous extracellular matrix in biomechanical properties of human skin model. Biofabrication, 2017, 9 (2), pp.025017. 10.1088/1758-5090/aa6ed5 . hal-01698349

HAL Id: hal-01698349

https://laas.hal.science/hal-01698349v1

Submitted on 24 Nov 2018

HAL is a multi-disciplinary open access archive for the deposit and dissemination of scientific research documents, whether they are published or not. The documents may come from teaching and research institutions in France or abroad, or from public or private research centers.

L'archive ouverte pluridisciplinaire **HAL**, est destinée au dépôt et à la diffusion de documents scientifiques de niveau recherche, publiés ou non, émanant des établissements d'enseignement et de recherche français ou étrangers, des laboratoires publics ou privés.

Importance of endogenous extracellular matrix in biomechanical properties of human skin model

Flavien Pillet[a]†, Laure Gibot[a]†, Moinecha Madi[a], Marie-Pierre Rols[a]*, Etienne Dague[b,c]*

[a] Institut de Pharmacologie et de Biologie Structurale, Université de Toulouse, CNRS, UPS, Toulouse, France

[b] Université de Toulouse III, 118 route de Narbonne, 31077 Toulouse, France

[c] LAAS-CNRS, 31400 Toulouse, France

†These authors contributed equally to this work

*Corresponding authors: Etienne Dague (edague@laas.fr)

Marie-Pierre Rols rols@ipbs.fr

LAAS, 7 avenue du colonel Roche, F-31400 Toulouse, France. Tel.: +33 561337841

ABSTRACT

The physical and mechanical properties of cells modulate their behavior such proliferation rate, migration and extracellular matrix remodeling. In order to study cell behavior in a tissue-like environment *in vitro*, it is of utmost importance to develop biologically and physically relevant 3D cell models. Here, we characterized the physical properties of a single cell type growing in configurations of increasing complexity. From one human skin biopsy, primary dermal fibroblasts were isolated and seeded to give monolayer (2D model), spheroid (3D model poor in extracellular matrix) and tissue-engineered cell sheet (3D model rich in endogenous extracellular matrix). Living native human dermis tissue was used as a gold standard. Nanomechanical and viscoelastic properties at the cell scale were measured by Atomic Force Microscopy (AFM) while biphoton microscopy allowed collagen detection by second harmonic generation and scanning electron microscopy helped in model morphological characterization. In all models, fibroblasts presented a similar typical elongated cell shape, with a cytoskeleton well-arranged along the long axis of the cell. However, elastic moduli of the tissue-engineered cell sheet and native dermis tissue were similar and statistically lower than monolayer and spheroid models. We successfully carried out AFM force measurements on 3D models such as spheroids and tissue-engineered cell sheets, as well as on living native human tissue. We demonstrated that a tissue-engineered dermal model recapitulates the mechanical properties of human native dermal tissue unlike the classically used monolayer and spheroid models. Furthermore, we give statistical evidence to indicate a correlation between cell mechanical properties and the presence of collagens in the models studied.

Key words: 2D, 3D, AFM, cell sheet, collagen, fibroblast, tissue engineering, self-assembly, spheroid

INTRODUCTION

Over the past century, cells cultured in two dimensions (2D) on glass or in Petri dishes served as an invaluable tool in cell biology [1]. Although still widely used and useful, growing cells in flat 2D monolayers on plastic surfaces does not accurately model the *in vivo* state. Nowadays, it is well accepted that 3D cell culture models are more relevant to *in vivo* situations than 2D cell cultures [2–6]. Indeed, 3D cell models exploit more representative spatial, biological, biochemical and biophysical parameters to bridge the gap between *in vitro* and *in vivo* experiments [7–9]. In addition, the presence of extracellular matrix in - 3D models is more relevant ,to mimic biochemical and biomechanical properties of cells within tissues [10,11].

Tissue engineering approaches have been widely used *in vitro* to produce 3D tissue equivalents, especially for skin substitutes [12,13]. Most of these methods rely on the use of biomaterials to provide a 3D structure, or scaffold, in which living cells are added. For example, fibroblasts, which are the main cell type within the dermis, can be embedded in different types of gel [14]. Although easy to carry out, this method presents some limitations. Fibroblasts seeded within collagen gels remodel them, leading to the phenomenon of collagen matrix contraction [15,16], making long-term culture unfeasible. By contrast, scaffold-free tissue-engineering approaches are based on the ability of cells to develop cell-cell interactions and to produce their own endogenous extracellular matrix. Spheroids were developed in the 1980s by Sutherland *et al*. and are based on cell aggregation properties when cells are cultured in suspension or in a non-adhesive environment [17]. Nowadays, spheroids are widely used *in vitro* to investigate many aspects of cell biology, especially in cancer studies [18,19]. However, some studies showed only a weak presence of extracellular matrix within spheroids [20,21]. The self-assembly approach is an attractive tissue-engineered strategy to produce *in vitro*, complex 3D tissue models rich in endogenous extracellular matrix [22]. The

reconstructed tissue produced by the self-assembly technology is called a cell sheet. Thus, it becomes possible to produce reconstructed human dermal tissue, devoid of any exogenous material [23–25]. We previously demonstrated that the primary human dermal fibroblasts reproduce a physiological environment by secreting and organizing a dense, native 3D extracellular matrix rich in organized collagens [26].

In this study, we analyzed the biophysical properties of human dermal fibroblasts grown under configurations of increasing complexity, going from a 2D classical monolayer to living native tissue. For this, we used a cutting edge multiparametric atomic force microscopy (AFM) in liquid which is particularly relevant to perform, morphological and mechanical analyses on live cells and useful to study cell interface properties in various areas, such as in microbiology, pharmacology and oncology [27–29]. However, while performing AFM experiments on cell monolayers is widespread, to the best of our knowledge we were the first to succeed in measuring mechanical forces by AFM in physiologic conditions, on a spheroid model, cell sheet model and fresh native tissue. Hence, our AFM experiments represented a technical challenge. Scanning Electron Microscopy (SEM) was used to characterize structural organization and architecture of the fibroblasts within the different models. Then, second harmonic generation (SHG) was used to visualize by two-photon microscopy, the organization of fibrillary collagens within extracellular matrix [30].

Our results provide a better understanding of the biophysical organization of each model presented in the next sections.

RESULTS

Cell morphological characterization.

Living human primary dermal fibroblasts seeded in distinct growth configurations were observed by optical microscopy during AFM measurements (Fig. 1). Fibroblasts seeded in monolayers appeared elongated and well spread out (Fig. 1a). Spheroids displayed a round shape with an average diameter of 250µm (Fig. 1b). Interestingly, no spheroids were taken off during AFM measurements by the passage of the tip. No artifacts with AFM tip were observed (Supplementary Fig.S1). Fibroblasts in cell sheets were narrower than those in monolayers (Fig. 1c). They grew in an orientated manner, parallel to each other. No picture of fresh native dermis could be taken as light was unable to pass through the thick tissue. Scanning electron microscopy gave a better definition of each model at cell scale (Fig. 2). In all models, fibroblasts were bipolar and elongated. At higher resolution (images of 10 µm x 10 µm), cytoskeleton was detectable under the cell surface in all cell models. The cell surface was smooth and no collagen fibers being observed either in monolayers (Fig. 2a) or in the spheroid model (Fig. 2b), whatever the magnification. In the cell sheet model (Fig. 2c) and native dermis tissue (Fig. 2d), cells were embedded in a complex extracellular matrix and were partially covered by large collagen fibers.

Topographic properties of fibroblasts within models of increasing complexity.

Quantitative Imaging measurements were performed by AFM to study the morphology in living conditions of various models of human dermal fibroblast. Height AFM images exhibited fibroblast cells from different growth configurations (Fig. 3). For monolayer (Fig. 3a), spheroid (Fig. 3b) and cell-sheet models (Fig. 3c), cells displayed distinct edges, a smooth surface and had a bipolar, elongated shape. Unfortunately, due to its heterogeneous

surface, no 50 µm x 50 µm pictures was acquired for the dermis tissue, so no conclusion can be reach on global fibroblast shape within this model. Interestingly, in higher resolution images (images of 10 µm x 10 µm), fibers were observed in the whole region of the cell well-arranged along the long axis of the cell, as previously shown for dermal fibroblasts [31]. Similar fibers were also observed in native dermis (Fig. 3d). These observations confirmed the typical fibroblast morphology for all the in vitro cell models studied.

Cytoskeleton motifs revealed by elasticity measurements.

Comparative topographic and elasticity studies were carried out by AFM to investigate the cytoskeleton of cells in a monolayer configuration, spheroid, tissue-engineered cell sheet and native dermis (Fig. 4). Quantitative data were obtained by scanning the area shown in the height AFM images (Fig. 4 a). 139478 curves were recorded, translated into elasticity maps given in Young's Modulus values at 200 nm depth (Fig. 4b), down to 1000 nm (data not shown). In all models, repetitive parallel motifs of cytoskeleton were noted in the cross section of Young's Modulus versus distance (Fig. 4c). Analysis by fast Fourier transform and filtering highlights the motifs (Fig. 4d). It confirmed the parallel stiff motifs with a periodicity between 0.7 and 1.2 µm. This observation suggests that the motifs visualized correspond to cytoskeleton, as previously described by AFM in dermal fibroblasts grown in a monolayer [31] and observed by fluorescent microscopy in Supplementary Fig. S2.

Cell membrane viscoelastic properties are correlated with collagen within the model.

For each model, the Young's Modulus values were calculated at 500 nm and 1000 nm of indentation from all the force curves (e.g. 36 780 curves from 9 maps in 3 independent monolayers, 53 246 curves from 13 maps in 3 independent spheroids, 36 466 curves from 9 maps in 3 independent cell-sheets and 12 986 curves from 6 maps in native dermis) and

expressed as histograms (Fig. 5ab). Statistical analyses (Table 1) revealed 2 groups of Young's Modulus, a group of low elasticity (around 50 Pa) corresponding to dermis and cell-sheet configurations and a group of higher elasticity (between 100 and 175 Pa) corresponding to spheroid and monolayer configurations. Interestingly, old monolayers grown for 4 weeks without ascorbic acid were also statistically significantly different to the cell-sheet (Supplementary Fig. S3). Multiphoton imaging was used. This non-invasive technology allows at high-resolution imaging of organized fibrillar collagen structures in living models. Monolayer and spheroid models showed a lack of SHG signal (Fig. 5cd), which confirms results observed by scanning electron microscopy (Fig. 2ab). Cell sheets and native dermis were highly positive for SHG (Fig. 5ef), meaning that organized fibrillar collagens were abundant in these models, as previously observed by SEM (Fig. 2 cd) and by histological analyses of tissue cross sections (Supplementary Fig. S4). Collagen content in each cell model was quantified with Imaris software (Supplementary Fig. S5). Thus, collagens represent 0 ± 0.0% of monolayer's volume, 0 ± 0.0% of spheroid's volume, 7 ± 1.4 of cell sheet's volume and 6 ± 2% of native dermis's volume.

DISCUSSION

Extracellular matrix mechanical properties synergize with chemical cues to drive cell behavior in culture and acts to establish and maintain tissue homeostasis *in vivo* [32]. Indeed, extracellular matrix was previously thought to serve only a structural and mechanical role by maintaining tissue architecture and providing a support for cell migration. However, nowadays it is recognized that it also provides biomechanical cues influencing a wide range of cell activities (adhesion, differentiation, phenotypic modulation, survival) [10]. Understanding tissue homeostasis requires now an appreciation of cell and tissue level mechanics and is an absolute necessity when designing therapies to treat cancers, chronic diseases or delayed wound healing. Thus, correlating confocal microscopy and atomic force indentation reveals that metastatic cancer cells stiffen during invasion into collagen [33]. AFM applied on sectioned mice-skin enables the connection of the tissue function to the corresponded ultrastructure and revealed tissue structures with a nanoscale resolution, especially in a wound model [34].

It is of utmost importance to develop relevant *in vitro* models providing biomechanical cues. By using cutting-edge advanced microscopies, we examined morphological and mechanical properties of human dermal fibroblasts grown in various cell models, compared to native human dermis tissue.

Our experiments SEM experiments revealed that the cell sheet is the closest model to human dermis, especially in terms of extracellular matrix content. We assumed that the extracellular matrix was mainly composed by fibrillar type I collagen, which is biosynthesized and remodeled by dermal fibroblasts [35] Highly organized collagen fibrils and fibers are known to provide skin its structural framework and mechanical properties [36] Interestingly, a correlation between extracellular matrix, gene expression and cell elasticity was recently described by Kim *et al* in human dermal fibroblast monolayers [31] They showed that a

decrease in pro-collagen I mRNA with cell aging is correlated with increased stiffness of dermal fibroblasts.

In conclusion, we investigated and proved the feasibility of carrying out AFM force measurements on 3D models such as spheroids and tissue-engineered cell sheets, as well as on living native human tissue. We demonstrated that cell mechanical properties depend on the cell growth configuration and overall on the presence of extracellular matrix. We underlined the major role of collagens on cell mechanical properties and proved that the tissue-engineered cell sheet model rich in collagens is the closest model to human native dermis. Within context, further experiments should be done to understand the impact of extracellular matrix on various cellular fates, such as proliferation, migration and differentiation but also to investigate its impact both on genes and proteins expression in skin fibroblasts.

Although there are an increasing number of studies published on the relevance of 3D models compared to classical 2D monolayers, their incomplete physical, mechanical and biochemical characterization limits their full potential exploitation.

Our observations offer perspectives in wound healing and aging studies with the relevant cell sheet model. Furthermore, developing relevant 3D cell culture models *in vitro* both from a biological and physical point of view complies with the ethical principles of animal research (3R's philosophy) by proposing alternative methods to the use of laboratory animals.

MATERIAL AND METHODS

Dermis native tissue and human cell isolation. Primary human dermal fibroblasts were isolated from a 3-year-old child's foreskin purchased from Icelltis (Toulouse, France) as previously described [23]. Briefly, after overnight incubation in Dispase II enzyme (10 mg/ml, Gibco-Invitrogen, Carlsbad, USA), epidermis was carefully peeled-off, and part of the fresh native dermis was used for direct analyses by AFM while another part was used for enzymatic isolation of fibroblasts with collagenase type 1 (1 mg/ml, Abnova, Taipei, Taiwan). 5 days after primary fibroblast isolation and expansion, cells at precocious passage 1, from the same batch, were used to seed and produce at least three independent monolayers, spheroids and cell sheet models. Cells were grown in Dulbecco's Modified Eagle's Medium (Invitrogen), supplemented with 10% of heat-inactivated fetal calf serum, 100U/ml penicillin and 100 µg/ml streptomycin. Cells were maintained at 37°C in a humidified atmosphere containing 5% CO_2.

Monolayer. For monolayers, cells were directly seeded (3 000 cells/cm²) onto removable, gelatin-coated 1-well Lab-tek glass slide (Fisher Scientific, Illkirch, France). Gelatin-coating allows better cell attachment and spreading. Three distinct cell monolayers were analyzed 5 days after seeding. Alternatively, cells grown in monolayer were cultivated for 4 weeks in order to compare their properties with cell sheet model.

Spheroid. We took advantage of our expertise in spheroid culture to include it in this comparative cell model study. Spheroids were generated by the non-adherent technique as previously described [37,38]. Briefly, 10 000 cells/well were seeded on ultra-low attachment

96-well plates (Fisher Scientific). At least three distinct spheroids were analyzed 5 days after seeding.

Cell sheet. Primary fibroblasts at passage 1 were seeded (15 000 cells/cm^2) onto 24-well plates as for monolayer, but grown for 4 weeks in complete cell culture medium supplemented with 50 µg/mL ascorbic acid (Sigma). When stimulated with vitamin C, cells are able to produce and assemble more collagen in the extracellular space. This trick is widely used in tissue engineering to produce tissue substitute by the self-assembly approach [22]. Indeed ascorbic acid, which is a co-factor of prolyl-hydroxylase and lysyl- hydroxylase enzymes, is well known to improve collagen production, secretion and maturation [39,40]. Three distinct cell sheets were analyzed 4 weeks after seeding.

Scanning electron microscopy. Cells were fixed with 2% glutaraldehyde in 0.1M Sorensen phosphate buffer pH7.2. The samples were prepared by the CMEAB platform (Toulouse, France). Images were visualized with an electron microscope QuantaTM 250 FEG (FEI, USA) at an accelerating voltage of 5 kV.

Atomic Force Microscopy. All AFM experiments were carried out in Phosphate Buffered Saline (Sigma-Aldrich) which is compatible with cell survival for at least 30min, as previously described by Chopinet *et al* [41]. AFM acquisitions lasted less than 15 min for each sample. For monolayers, cells were directly observed on gelatin-coated Lab-tek glass slide. Spheroids were immobilized for 15 min on a glass slide coated with polyethylenimine (PEI) (Sigma-Aldrich). Cell sheet and native dermis were directly deposited on the glass slide. AFM measurements were performed with a Nanowizard III (JPK Instruments, Germany) in

Quantitative Imaging mode (QI) [42]. The cantilever (CP-PNPL NanoAndMore) spring constant was measured by the thermal tune method [43] before each experiment and found to lie in the range of 0.05N/m to 0.2N/m. A force of 10 nN was applied. The loading frequency was 100 Hz and the indentation speed 400 µm/s, as used in previous studies [44]. Cell elasticity was determined from the Young's Modulus values which were calculated with the JPK Data processing software (JPK) from square QI images of 10 µm using the Hertz Model [45,46] and according to the equation 1. Typical force distance curved used for Young's Modulus calculations were shown in Fig. 6.

Equation 1: $F = \frac{4}{3} \cdot \frac{E}{1-\upsilon_s^2} \cdot \sqrt{r} \cdot \delta^{\frac{3}{2}}$

Where F is the applied force in N, E the Young's Modulus in Pa, υ_s Poisson's ratio, r the tip radius of the probe in m and δ the indentation of the sample in m. Here, we considered AFM tip as a sphere of 10 µm of radius and a Poisson ratio of 0.5 was applied.

Elasticity maps were obtained at 200 nm depth, as previously described in the literature [47,48]. Fast Fourier Transform (FFT) calculations were carried out with the free software Gwyddion 2.41.

Statistical analysis The elasticity maps were obtained by calculation of the Young's Modulus values which were deduced from each approach curve (Fig. 6). The statistical analyses between each cell model were performed from the means of elasticity maps and by using the non-parametric Mann-Whitney test with the Prism5.04 software (GraphPad).

Collagens detection by second harmonic generation (SHG). As previously described [26], 3D stacks of 425x425x60 µm were acquired using a 7MP multiphoton laser scanning microscope (Carl Zeiss, Jena, Germany), equipped with a 20x objective and coupled to a Ti-sapphire femtosecond laser, Chameleon Ultra 2 (Coherent Inc) tuned to 800 nm. Organized fibrillar collagens were detected by second harmonic generation at a wavelength of 400 nm. The acquired 3D images and collagens quantification were analyzed off-line with Imaris software (Bitplane AG). Briefly the volume occupied by the collagen was calculated by measuring the volume occupied by the isosurface of the SHG in a cube of defined volume (80,1 x 80,1 x 80 µm). Three independent samples were used for each condition.

Histological staining

Fresh cell sheets and native dermis tissues were embedded in OCT and conserved at -80°C until use. 5µm sections were realized on a cryostat. After removal of OCT in deionized water, tissue sections were stained with Masson's trichrome according to the manufacturer's protocol (Sigma-Aldrich). The Masson's trichrome method stains cells red and collagens within the dermal tissue in blue [49].

ACKNOWLEDGEMENTS

This research was performed in the scope of the EBAM European Associated Laboratory (LEA) and is a result of networking efforts within COST TD1104. We were supported by the Centre National de la Recherche Scientifique (CNRS), the Agence Nationale de la Recherche (ANR), Projet PIERGEN ANR-12-ASTR-0039, the Direction Générale de l'Armement (DGA), the Midi-Pyrénées Région and the Fondation d'entreprise SILAB-Jean Paufique. Microscopy experiments were carried out on the Plateforme Genotoul Toulouse RIO Imaging. The authors would like to gratefully acknowledge Elisabeth Bellard (IPBS), Isabelle Fourquaux (CMEAB) for their technical assistance in imaging experiments, and the late Mr Peter Winterton, a native English scientist, for his careful proofreading of this manuscript.

REFERENCES

[1] Carrel A 1912 On the permanent life of tissues outside of the organism *J Exp Med* **15** 516–28

[2] Schmeichel K L and Bissell M J 2003 Modeling tissue-specific signaling and organ function in three dimensions *J Cell Sci* **116** 2377–88

[3] Schwartz M A and Chen C S 2013 Deconstructing Dimensionality *Science* **339** 402–4

[4] Yamada K M and Cukierman E 2007 Modeling tissue morphogenesis and cancer in 3D *Cell* **130** 601–10

[5] Abbott A 2003 Cell culture: biology's new dimension *Nature* **424** 870–2

[6] Abbott R D and Kaplan D L 2015 Strategies for improving the physiological relevance of human engineered tissues *Trends Biotechnol.* **33** 401–7

[7] Pampaloni F, Reynaud E G and Stelzer E H K 2007 The third dimension bridges the gap between cell culture and live tissue *Nature Reviews Molecular Cell Biology* **8** 839–45

[8] Smalley K S M, Lioni M and Herlyn M 2006 Life isn't flat: taking cancer biology to the next dimension *In Vitro Cell. Dev. Biol. Anim.* **42** 242–7

[9] Leong D T and Ng K W 2014 Probing the relevance of 3D cancer models in nanomedicine research *Adv. Drug Deliv. Rev.* **79**–**80** 95–106

[10] Humphrey J D, Dufresne E R and Schwartz M A 2014 Mechanotransduction and extracellular matrix homeostasis *Nat Rev Mol Cell Biol* **15** 802–12

[11] Wang N, Tytell J D and Ingber D E 2009 Mechanotransduction at a distance: mechanically coupling the extracellular matrix with the nucleus *Nature Reviews Molecular Cell Biology* **10** 75–82

[12] Langer R and Vacanti J P 1993 Tissue engineering *Science* **260** 920–6

[13] Badylak S F, Weiss D J, Caplan A and Macchiarini P 2012 Engineered whole organs and complex tissues *Lancet* **379** 943–52

[14] Hakkinen K M, Harunaga J S, Doyle A D and Yamada K M 2011 Direct comparisons of the morphology, migration, cell adhesions, and actin cytoskeleton of fibroblasts in four different three-dimensional extracellular matrices *Tissue Eng Part A* **17** 713–24

[15] Elsdale T and Bard J 1972 Collagen substrata for studies on cell behavior *J. Cell Biol.* **54** 626–37

[16] Grinnell F and Petroll W M 2010 Cell motility and mechanics in three-dimensional collagen matrices *Annu. Rev. Cell Dev. Biol.* **26** 335–61

[17] Sutherland R M and Durand R E 1984 Growth and cellular characteristics of multicell spheroids *Recent Results Cancer Res.* **95** 24–49

[18] Hirschhaeuser F, Menne H, Dittfeld C, West J, Mueller-Klieser W and Kunz-Schughart L A 2010 Multicellular tumor spheroids: an underestimated tool is catching up again *J. Biotechnol.* **148** 3–15

[19] Nyga A, Cheema U and Loizidou M 2011 3D tumour models: novel in vitro approaches to cancer studies *J Cell Commun Signal* **5** 239–48

[20] Nederman T, Norling B, Glimelius B, Carlsson J and Brunk U 1984 Demonstration of an extracellular matrix in multicellular tumor spheroids *Cancer Res.* **44** 3090–7

[21] Santini M T, Rainaldi G and Indovina P L 2000 Apoptosis, cell adhesion and the extracellular matrix in the three-dimensional growth of multicellular tumor spheroids *Crit. Rev. Oncol. Hematol.* **36** 75–87

[22] Athanasiou K A, Eswaramoorthy R, Hadidi P and Hu J C 2013 Self-organization and the self-assembling process in tissue engineering *Annu Rev Biomed Eng* **15** 115–36

[23] Gibot L, Galbraith T, Huot J and Auger F A 2010 A preexisting microvascular network benefits in vivo revascularization of a microvascularized tissue-engineered skin substitute *Tissue Eng Part A* **16** 3199–206

[24] Gibot L, Galbraith T, Huot J and Auger F A 2013 Development of a tridimensional microvascularized human skin substitute to study melanoma biology *Clin. Exp. Metastasis* **30** 83–90

[25] Gibot L, Galbraith T, Kloos B, Das S, Lacroix D A, Auger F A and Skobe M 2016 Cell-based approach for 3D reconstruction of lymphatic capillaries in vitro reveals distinct functions of HGF and VEGF-C in lymphangiogenesis *Biomaterials* **78** 129–39

[26] Madi M, Rols M-P and Gibot L 2015 Efficient In Vitro Electropermeabilization of Reconstructed Human Dermal Tissue *J. Membr. Biol.*

[27] Formosa C, Pillet F, Schiavone M, Duval R E, Ressier L and Dague E 2015 Generation of living cell arrays for atomic force microscopy studies *Nat Protoc* **10** 199–204

[28] Pillet F, Chopinet L, Formosa C and Dague E 2014 Atomic Force Microscopy and pharmacology: from microbiology to cancerology *Biochim. Biophys. Acta* **1840** 1028–50

[29] Pillet F, Lemonier S, Schiavone M, Formosa C, Martin-Yken H, Francois J M and Dague E 2014 Uncovering by atomic force microscopy of an original circular structure at the yeast cell surface in response to heat shock *BMC Biol.* **12** 6

[30] Bancelin S, Aimé C, Gusachenko I, Kowalczuk L, Latour G, Coradin T and Schanne-Klein M-C 2014 Determination of collagen fibril size via absolute measurements of second-harmonic generation signals *Nat Commun* **5** 4920

[31] Kim K S, Park H-K, Lee J-W, Kim Y I and Shin M K 2015 Investigate correlation between mechanical property and aging biomarker in passaged human dermal fibroblasts *Microsc. Res. Tech.* **78** 277–82

[32] Gilbert P M and Weaver V M 2016 Cellular adaptation to biomechanical stress across length scales in tissue homeostasis and disease *Semin. Cell Dev. Biol.*

[33] Staunton J R, Doss B L, Lindsay S and Ros R 2016 Correlating confocal microscopy and atomic force indentation reveals metastatic cancer cells stiffen during invasion into collagen I matrices *Sci Rep* **6** 19686

[34] Chang A C, Liu B H, Shao P L and Liao J D 2017 Structure-dependent behaviours of skin layers studied by atomic force microscopy *J Microsc*

[35] Shoulders M D and Raines R T 2009 Collagen structure and stability *Annu. Rev. Biochem.* **78** 929–58

[36] Sherman V R, Yang W and Meyers M A 2015 The materials science of collagen *J Mech Behav Biomed Mater*

[37] Gibot L, Lemelle A, Till U, Moukarzel B, Mingotaud A-F, Pimienta V, Saint-Aguet P, Rols M-P, Gaucher M, Violleau F, Chassenieux C and Vicendo P 2014 Polymeric micelles encapsulating photosensitizer: structure/photodynamic therapy efficiency relation *Biomacromolecules* **15** 1443–55

[38] Gibot L, Wasungu L, Teissié J and Rols M-P 2013 Antitumor drug delivery in multicellular spheroids by electropermeabilization *J Control Release* **167** 138–47

[39] Lyons B L and Schwarz R I 1984 Ascorbate stimulation of PAT cells causes an increase in transcription rates and a decrease in degradation rates of procollagen mRNA *Nucleic Acids Res.* **12** 2569–79

[40] Schwarz R I 1985 Procollagen secretion meets the minimum requirements for the rate-controlling step in the ascorbate induction of procollagen synthesis *J. Biol. Chem.* **260** 3045–9

[41] Louise C, Etienne D and Marie-Pierre R 2014 AFM sensing cortical actin cytoskeleton destabilization during plasma membrane electropermeabilization *Cytoskeleton (Hoboken)* **71** 587–94

[42] Chopinet L, Formosa C, Rols M P, Duval R E and Dague E 2013 Imaging living cells surface and quantifying its properties at high resolution using AFM in QI™ mode *Micron* **48** 26–33

[43] Hutter J L and Bechhoefer J 1993 Calibration of atomic-force microscope tips *Review of Scientific Instruments* **64** 1868–73

[44] Smolyakov G, Formosa-Dague C, Severac C, Duval R E and Dague E 2016 High speed indentation measures by FV, QI and QNM introduce a new understanding of bionanomechanical experiments *Micron* **85** 8–14

[45] Hertz H 1881 Ueber die Berührung fester elastischer Körper. *Journal für die reine und angewandte Mathematik* **1882** 156–71

[46] Sen S, Subramanian S and Discher D E 2005 Indentation and adhesive probing of a cell membrane with AFM: theoretical model and experiments *Biophys. J.* **89** 3203–13

[47] Kasas S, Wang X, Hirling H, Marsault R, Huni B, Yersin A, Regazzi R, Grenningloh G, Riederer B, Forrò L, Dietler G and Catsicas S 2005 Superficial and deep changes of cellular mechanical properties following cytoskeleton disassembly *Cell Motil. Cytoskeleton* **62** 124–32

[48] Longo G, Rio L M, Roduit C, Trampuz A, Bizzini A, Dietler G and Kasas S 2012 Force volume and stiffness tomography investigation on the dynamics of stiff material under bacterial membranes *J. Mol. Recognit.* **25** 278–84

[49] Masson P 1929 Some histological methods; trichrome stainings and their preliminary technique **12** 75–90

FIGURES

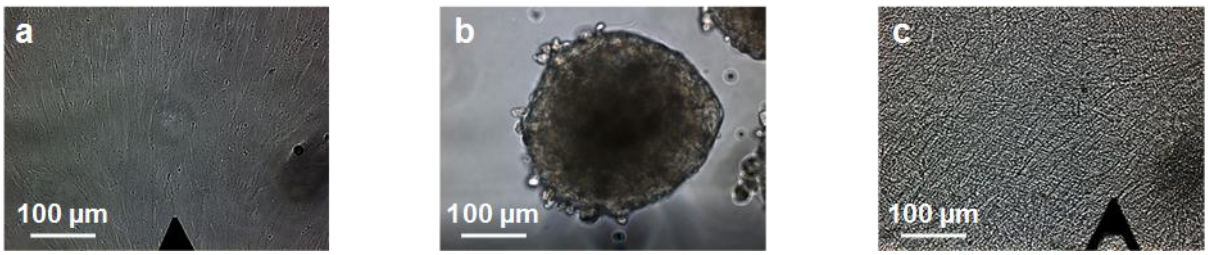

Figure 1. Optical pictures of human dermal fibroblast in various growth configurations. Pictures of fibroblast monolayer (a), spheroid (b) and cell sheet (c) taken during AFM experiments.

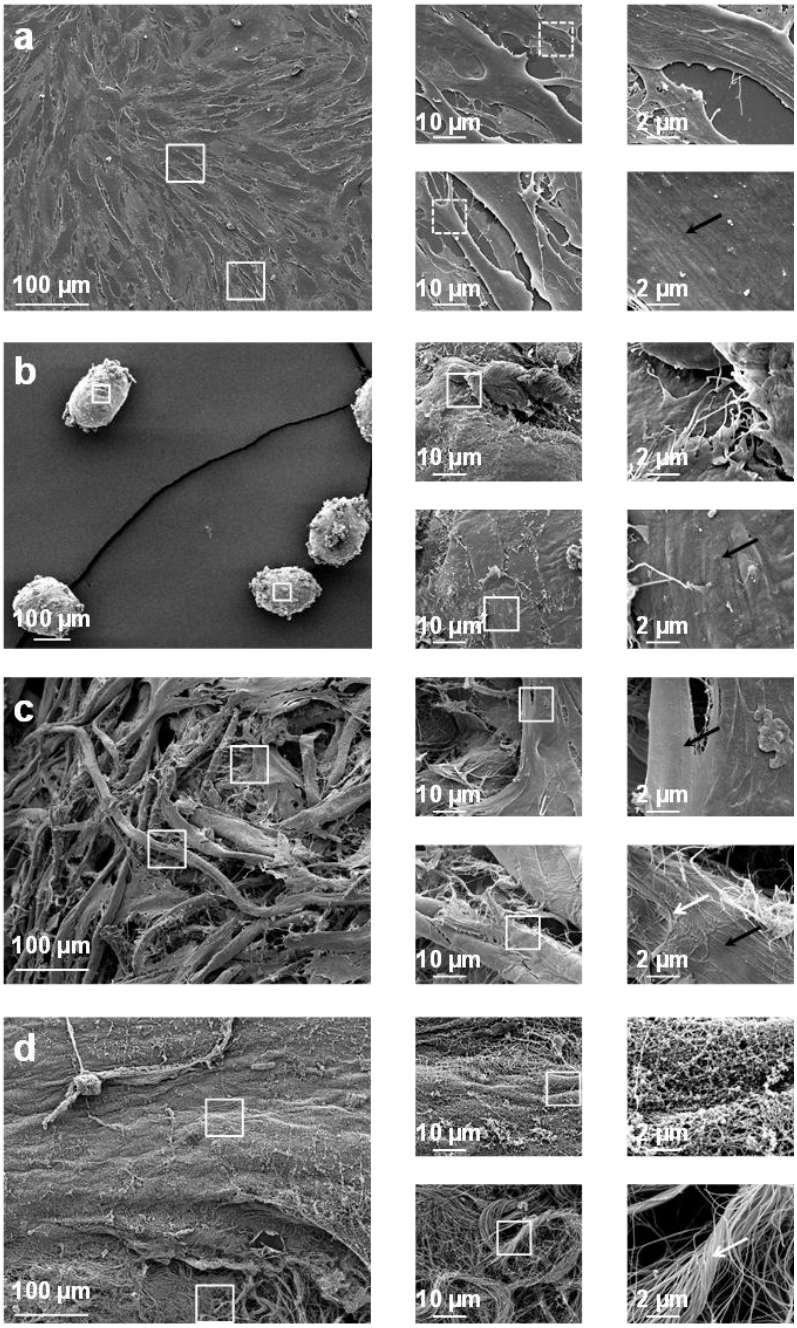

Figure 2. Scanning Electron Microscopy (SEM) pictures of cell models of increasing complexity from cell monolayer to native dermal tissue. SEM shows the cell architecture and organization in monolayer (a), spheroid (b), cell sheet (c) and native dermis (d). Inset exhibits the presence of naked cells on monolayer and spheroid and cell partially covered by collagens fibers on cell sheet and native dermis (white arrows). Black arrows indicate the cytoskeleton fibers.

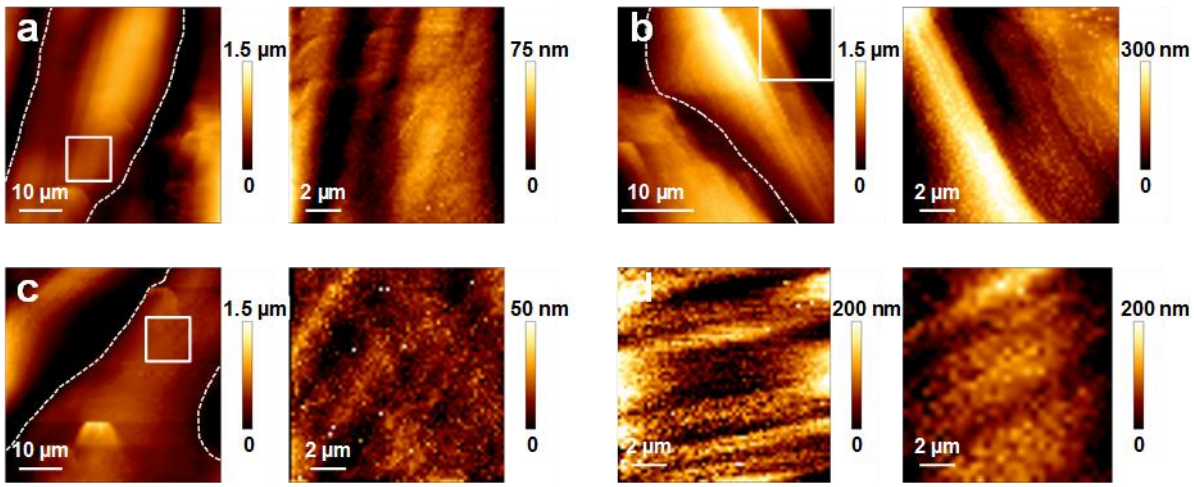

Figure 3. Atomic Force Microscopy (AFM) height images of cell models of increasing complexity. Examples of topographic images obtained by AFM on monolayer (a), spheroid (b), cell sheet (c) and native dermis (d). The dashed lines revealed the positions of individual cells.

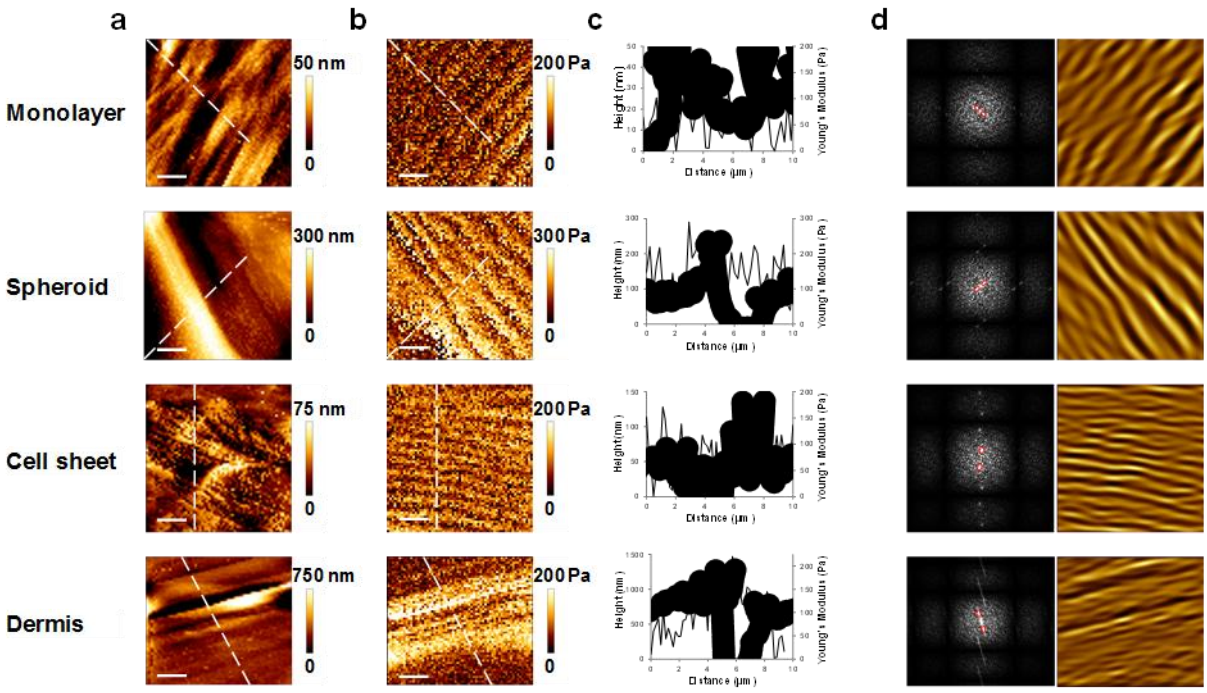

Figure 4. Visualization of the cytoskeleton motifs by AFM measurements. (a) Height images showed the surface morphology of cells. (b) Elasticity measurements on the same area revealed corresponding motifs for a depth of 200 nm. (c) Height (full lines) and elasticity (dotted line) cross sections were taken across the dashed lines in a and b. (d) Fourier transforms were obtained from elasticity maps. The filtering of Fourier Transform (red circles) exhibited the cytoskeleton motifs. Data were obtained from representative fibroblast cells in monolayer, spheroid, tissue-engineered cell sheet and native dermis. Scale bars: 2 µm.

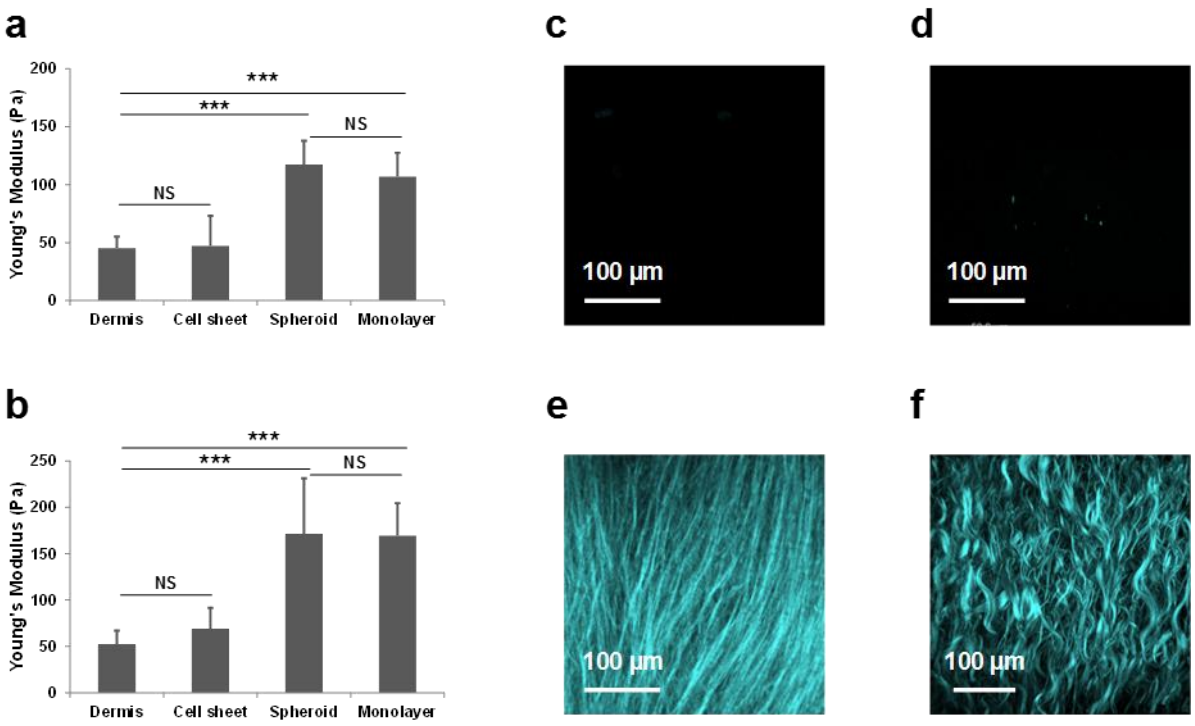

Figure 5. Relationship between global elasticity and collagens. Histograms of elasticity measurements at 500 nm (a) and 1000 nm (b) of deep. Examples of Second Harmonic Generation (SHG) indicating organized collagen fibers. Collagens are absent from monolayer (c) and spheroids (d). By contrast collagen was clearly detected on cell-sheet (e) and native dermis (f).

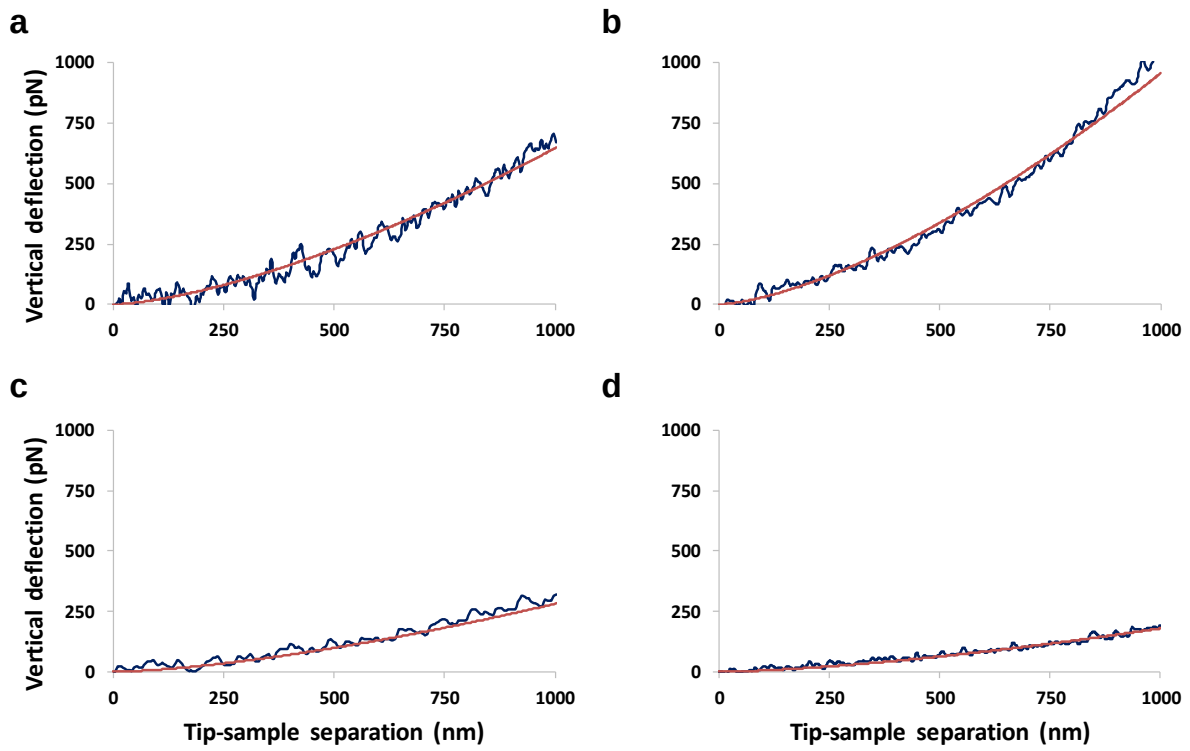

Figure 6. Examples of Force distance curved used for Young's Modulus calculations. The Young's Modulus were calculated with indentation curves (blue lines) on 1000 µm from monolayers (a), spheroid (b), cell sheet (c) and dermis (d). The Hertz fitted curves (red lines) were calculated from the Hertz model (equation 1).

Table 1. Statistical analyses of Young's Modulus revealed 2 groups of elasticity. For each model, the mean values of Young's Modulus were calculated at 500 nm and 1000 nm from the elasticity maps and their related curves. Non-parametric statistical analyses were performed with the Mann-Whitney test. 4!/4 pairs of test were performed to compare all the conditions with each other. The level of significance is given by the Pvalue (* for <0.05; ** for <0.01; *** for <0.001; **** for <0.0001)). Non-significant differences of Young's Modulus were obtained between the dermis and the cell-sheet and between the spheroids and the monolayer.

		Maps	Curves	Mean (Pa)	Statistical comparisons	Mann-Whitney test (P value)
500 nm indentation	Dermis	6	12978	46 ± 10	Dermis/Cell-sheet	0.3884
	Cell-sheet	9	36466	47 ± 26	Dermis/Spheroids	0.0007 ***
	Spheroid	13	53246	117 ± 20	Dermis/Monolayer	0.0004 ***
	Monolayer	9	36780	107 ± 21	Cell-sheet/Spheroids	0.0002 ***
					Cell-sheet/Monolayer	0.0003 ***
					Spheroids/Monolayer	0.4229
1000 nm indentation	Dermis	6	12978	52 ± 15	Dermis/Cell-sheet	0.0879
	Cell-sheet	9	36466	69 ± 23	Dermis/Spheroids	0.0007 ***
	Spheroid	13	53246	171 ± 60	Dermis/Monolayer	0.0004 ***
	Monolayer	9	36780	169 ± 35	Cell-sheet/Spheroids	0.0002 ***
					Cell-sheet/Monolayer	<0.0001 ****
					Spheroids/Monolayer	0.3853